Volume 52(11): 1415–1425, 2004
Journal of Histochemistry & Cytochemistry
http://www.jhc.org

ARTICLE

Immunolocalization of Caveolin-1 in Rat and Human Mesothelium

Christopher J. von Ruhland, Lee Campbell, Mark Gumbleton, Bharat Jasani, and Geoffrey R. Newman

Medical Microscopy Sciences, University of Wales College of Medicine (CJvR,GRN); Welsh School of Pharmacy, Cardiff University (LC,MG); and Department of Histopathology, University Hospital of Wales (BJ), Heath, Cardiff, Wales, United Kingdom

SUMMARY Flask-shaped vesicles have been described as caveolae in mesothelial cells in a number of animal species based on morphological criteria only. Using an antibody against caveolin-1, said to be a biochemical marker of caveolae, immunoelectron microscopy suggests that many but not all such vesicles in mesothelial cells are caveolae. Mesothelial cells from different anatomical sites showed obvious variations in both the population density and distribution of these flask-shaped vesicles and in their density of immunostaining. Lung and pericardial sac had the highest staining density. In some sites (e.g., lung, bladder, colon) caveolae were equally distributed between apical and basolateral surfaces, whereas in others (e.g., spleen, liver), they were predominantly apical. Additional immunopositive sites in the peritoneal membrane were identified, including the epineurium of peripheral nerves and the endothelium of lymphatic vessels. We further suggest that variations in the number of mesothelial cell caveolae and the density of their immunolabeling may have implications for our understanding of certain diseases such as malignant mesothelioma, especially in view of the recent hypothesis that it may be caused by SV40, a virus that appears to enter cells via caveolae. **(J Histochem Cytochem 52:1415–1425, 2004)**

KEY WORDS
caveolin-1
caveolae
immunoelectron microscopy
mesothelium
peritoneum

FINE PARIETAL AND VISCERAL MEMBRANES, respectively, cover the body's cavities and the organs that lie within them. These membranes comprise a sheet of squamous mesothelial cells overlying a layer of loose connective tissue containing blood vessels, lymphatics, nerves, fibroblasts, and occasional mast cells. In the thorax, the pleural membrane lines the cavity and envelops the lungs, and the pericardial membrane lines the pericardial sac and surrounds the heart. In the abdomen, the membrane is termed the peritoneum. These membranes provide a lubricating surface for the viscera and may be involved in host defense (Holmes 1994).

In the past two decades there has been increasing interest in mesothelial tissues, principally as a result of reports of the transformation of mesothelial cells from thoracic membranes by exposure to asbestos fibers (Craighead and Mossman 1982; Ke et al. 1989) and viruses (Cicala et al. 1993; Carbone et al. 1994; Bocchetta et al. 2000); such transformation can lead to malignant mesothelioma. In addition, the properties of the peritoneal membrane are of fundamental importance because it represents the dialyzing surface in patients receiving continuous ambulatory peritoneal dialysis (CAPD).

Caveolae, as defined by Yamada (1955), are 80–100-nm flask-shaped invaginations of the plasma membrane. They are observed morphologically in a wide variety of cell types, including, most prominently, microvascular endothelium (Simionescu and Simionescu 1983), fibroblasts (Bretscher and Whytock 1977), adipocytes, and smooth-muscle cells (Forbes et al. 1979), and have been described as noncoated vesicles due to their lack of the electron-dense cytoplasmic coat that is characteristic of plasmalemmal clathrin-coated pits.

Caveolae appear to perform a number of cellular functions, including serving as a localizing domain within the plasma membrane for a range of signal

Correspondence to: Christopher J. von Ruhland, Medical Microscopy Sciences, University of Wales College of Medicine, Heath, Cardiff CF14 4XN, UK. E-mail: vonruhlandcj@cf.ac.uk

Received for publication April 3, 2004; accepted June 1, 2004 [DOI: 10.1369/jhc.4A6334.2004].

0022-1554/04/$3.30

transduction molecules (Anderson 1999; Schlegel and Lisanti 2001), concentration and internalization of small molecules or ions by the process of potocytosis (Anderson et al. 1992), and involvement in intracellular trafficking (Fielding and Fielding 1996) and in endocytotic and transcytotic functions (Schnitzer et al. 1994), including serving as a portal for the entry of a range of microorganisms and toxins (Shin and Abraham 2001). Many of these functions are reliant to a lesser or greater extent on the caveolae marker protein and on the key structural and functional protein caveolin-1. The identification of caveolin-1 (a 22-kD integral membrane protein) as a major component of caveolar membranes (Glenney and Soppet 1992; Rothberg et al. 1992) has allowed these caveolar vesicles to be identified immunocytochemically in a variety of cells, such as fibroblasts (Rothberg et al. 1992; Smart et al. 1995), endothelial cells (Rajamannan et al. 2002), and type 1 pneumocytes (Newman et al. 1999).

Membrane vesicles morphologically characteristic of caveolae have long been described in mesothelial cells in a variety of species, including frog (Hama 1960), mouse (Ettarh and Carr 1996), and human (Slater et al. 1989). Intriguingly, changes in the number and size of such vesicles in peritoneal mesothelial cells have been documented in patients receiving CAPD (Dobbie and Zaki 1986; Dobbie 1989).

Given the multifunctional roles ascribed to caveolae and the different types of noncoated membrane vesicles present within cells, we sought in this study to use immunoelectron microscopy to localize caveolin-l to the non-coated vesicles in mesothelial tissue. Biochemical evidence that these structures are caveolae has broad implications for the functional assignment and further study of these structures in relation to mesothelial cell biology.

Materials and Methods

Rat Tissue

The paucity of normal human tissue necessitated the use of material from animal sources for preliminary optimization studies. Tissue was immersion fixed to maintain comparability with processing of human tissue samples. Separate animal tissue was fixed by perfusion to provide ideally preserved tissue.

Male pathogen-free Wistar rats (180–220 g) were used throughout. The rats were bred and maintained under controlled temperature and lighting with access to food and water ad libitum. Experiments were conducted in accordance with the Animal (Scientific Procedures) Act of 1986.

Immersion Fixation

For immersion fixation, animals were terminally anesthetized with halothane and sacrificed under schedule 1. The pleural, pericardial, and peritoneal cavities were opened and flooded with 100 mM sodium phosphate buffer, pH 7.4, plus 2% (w/v) sucrose (sample buffer) containing 4% formaldehyde plus 0.2% glutaraldehyde (sample fixative). After 15 min, tissue specimens were collected from body cavity walls and organs and immersion fixed for a further 24 hr in sample fixative. The fixed samples were washed with several changes of sample buffer to remove excess fixative and were stored at 4C before further processing.

Perfusion Fixation

After terminal anesthesia with halothane, a canula was immediately inserted into the aorta at a site distal to the pulmonary artery, and a bolus (100 μl) of 0.1% (w/v) $NaNO_2$ was administered. The vasculature was perfused with balanced saline solution followed by 15-min perfusion with 1% (v/v) glutaraldehyde in 100 mM sodium phosphate buffer, pH 7.3 (Yoshimura et al. 1986). Tissue samples were collected and immersion fixed for a further 45 min by immersion in the same fixative. Samples were washed with several changes of sample buffer to remove excess fixative and were stored at 4C before further processing.

Human Tissue

Human parietal peritoneum was excised from consenting patients undergoing donor nephrectomy using a trauma-free, knotted suture method (von Ruhland et al. 2003). Briefly, a suture was inserted into the external surface of the peritoneum and the membrane raised above the viscera. A sample of tissue (1.5 cm about the suture) was excised and briefly placed in sample buffer before being pinned onto a silicone elastomer surface (Sylgard 184; VWR International, Lutterworth, UK) (submerged in sample buffer) with the mesothelial surface uppermost. The sample buffer was poured away, and the tissue was then flooded with sample fixative for 15 min at room temperature. The tissue was carefully removed from the silicone elastomer and fixed for 24 hr in sample fixative at room temperature. After several washes in sample buffer, the tissue was stored at 4C before further processing.

Tissue Processing

Strips of tissue 5 mm × 1 mm were postfixed for 2 hr in 2% (w/v) aqueous uranyl acetate, partially dehydrated in ethanol [30 min in 50% (v/v), twice for 30 min in 70% (v/v)], infiltrated with LR White acrylic resin (London Resin Company; Reading, UK) (45 min in 2:1 LR White/70% ethanol, four times for 1 hr in neat resin, all at 4C), and polymerized by the cold chemical catalytic technique (Newman and Hobot 2001). For electron microscopy, thin (80–100-nm) resin sections were mounted unsupported on the shiny side of ethanol-washed 300-mesh nickel grids and allowed to air dry.

For light microscopy, semithin (0.35 μm) resin sections were floated onto droplets of ddH_2O on Vectabond (Vector Laboratories; Peterborough, UK)-treated slides and dried for 2 hr in an oven at 50C. Rodent membranes were not studied at the light microscopic level because they are exceptionally thin, comprising only mesothelial cells and underlying collagen containing occasional fibroblasts.

Immunocytochemistry

Thin Resin Sections. Grids were equilibrated twice for 10 min in 50-μl drops comprising 0.6% bovine serum albumin

in 20 mM Tris-buffered saline, pH 7.4 (TBS/BSA). Grids were then incubated for 1 hr in 50-μl drops of rabbit anti-caveolin-1 polyclonal antibody (BD Biosciences; Cowley, UK) at dilutions of 1:500, 1:1000, 1:2000, or 1:4000 in TBS/BSA. After incubation, grids were washed three times for 1 min in 50-μl drops of TBS/BSA and then incubated for 1 hr in 50-μl drops of goat anti-rabbit IgG–10-nm colloidal gold conjugate (manufactured in-house) in TBS/BSA. Grids were then rinsed in 50-μl drops of TBS/BSA for 1 min and in ddH_2O twice for 1 min before counterstaining with 2% uranyl acetate and Reynolds lead citrate.

For double immunolabeling of human tissue, grids were immunostained as above, except that the droplets of primary antibody contained both rabbit anti-caveolin-1 polyclonal antibodies, and mouse anti-vimentin (DakoCytomation; Ely, UK) monoclonal antibodies, and the drops of secondary antibody-colloidal gold conjugate contained both goat anti-rabbit IgG–10-nm colloidal gold conjugate and goat anti-mouse-20-nm colloidal gold conjugate.

Sections were examined in a Philips CM12 transmission electron microscope at 80 kV. Photographic plates were digitally imaged with a UMAX Powerlook III scanner (UMAX Data Systems; Taipei, Taiwan, ROC) and processed with Adobe Photoshop (Adobe Systems; San Jose, CA).

Semithin Resin Sections. Sections of human parietal peritoneum were equilibrated twice for 10 min with TBS/BSA, after which they were incubated for 1 hr at room temperature in serial dilutions (1:500, 1:1000, 1:2000, and 1:4000) of rabbit anti-caveolin-1 polyclonal antibody in TBS/BSA. Sections were then washed three times for 1 min with TBS/BSA and incubated for 1 hr with 100-μl droplets of goat anti-rabbit Ig-10-nm colloidal gold conjugate in TBS/BSA. Sections were washed in TBS/BSA for 1 min and in ddH_2O

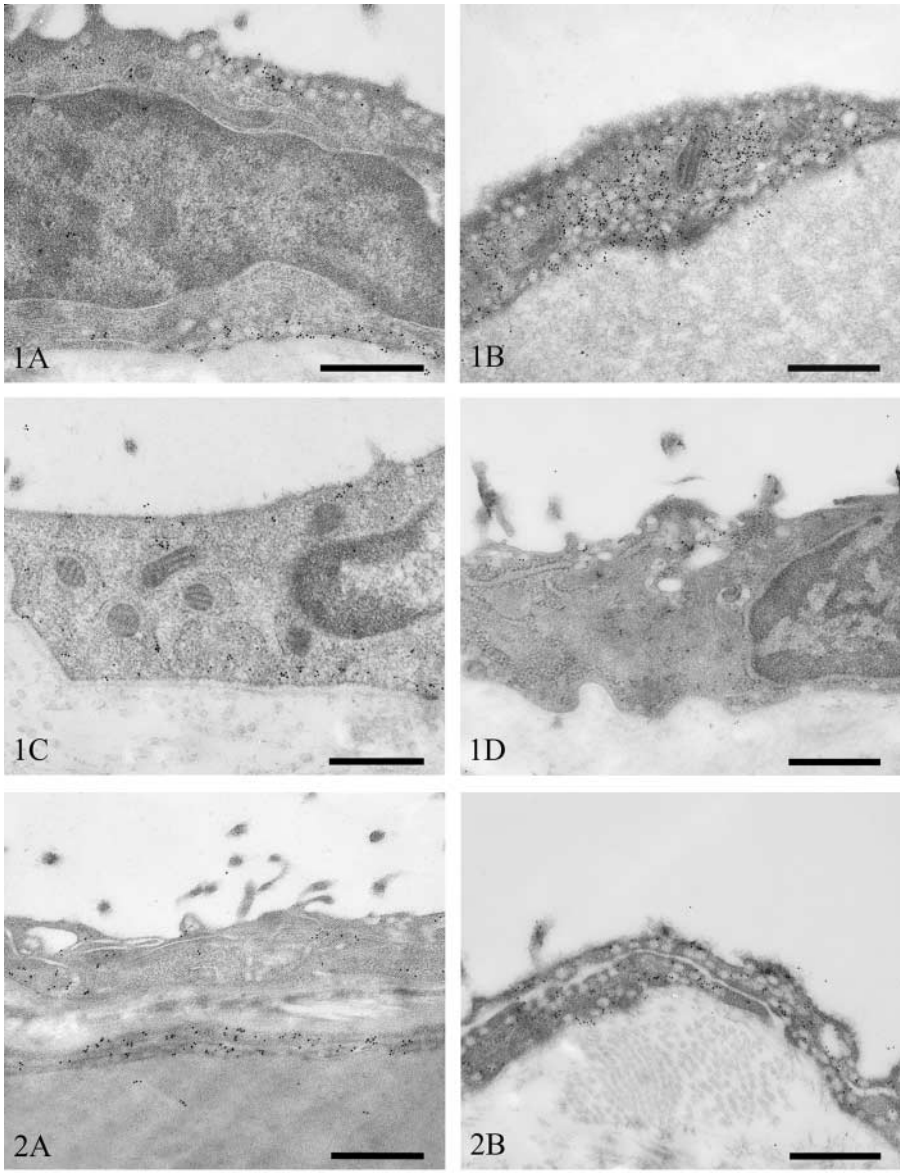

Figure 1 Transmission electron micrographs of rat pleural mesothelium immunostained for caveolin-1. Lung mesothelium showing apical and basolateral vesicular staining (**A**) and dense foci of immunopositive vesicles (**B**). Diaphragm (**C**) and intercostal muscle (**D**). Bars = 500 nm.

Figure 2 Transmission electron micrographs of rat pericardial mesothelium immunostained for caveolin-1. Heart (**A**) and pericardial sac (**B**). Bars = 500 nm.

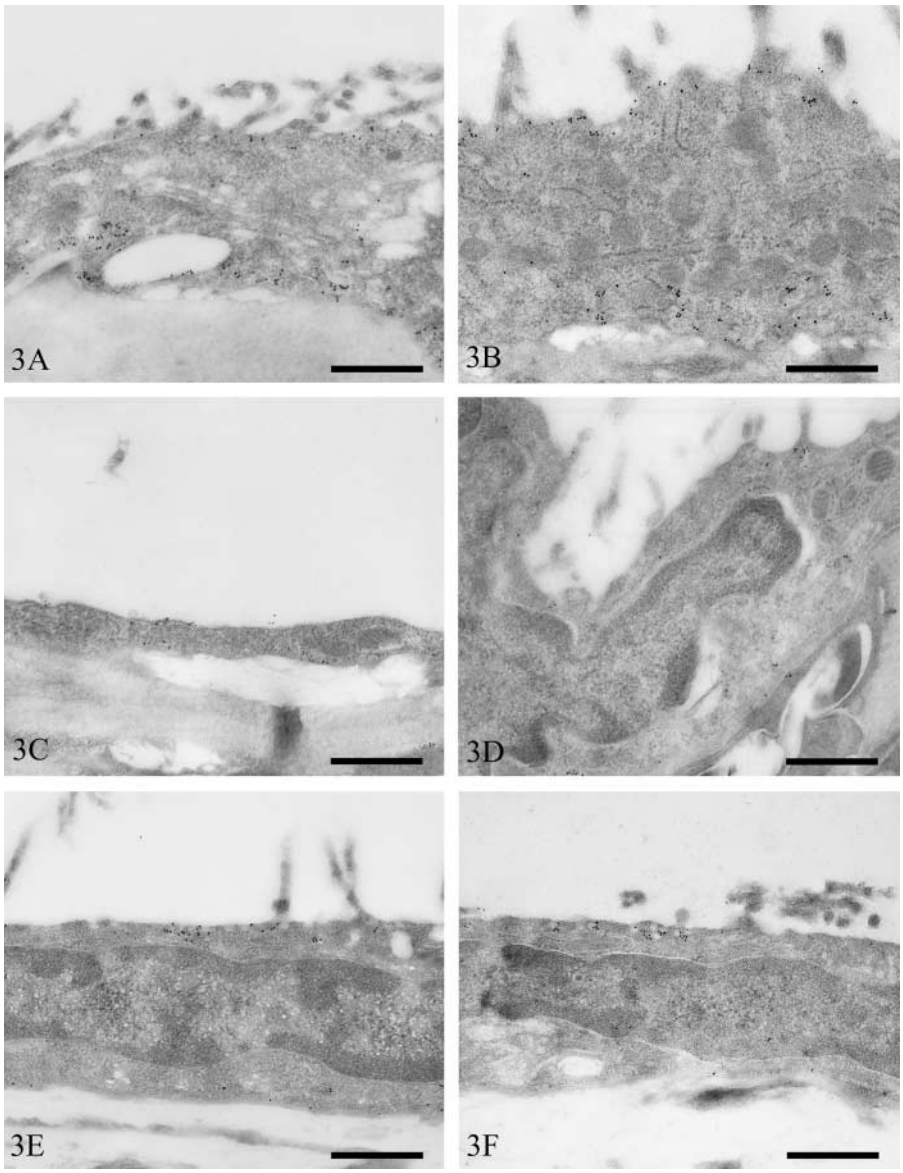

Figure 3 Transmission electron micrographs of rat peritoneal mesothelium immunostained for caveolin-1. Bladder (**A**), colon (**B**), kidney (**C**), duodenum (**D**), spleen (**E**), liver (**F**), mesentery (**G**), pancreas (**H**), stomach (**I**), and abdominal wall (**J**). Bars = 500 nm.

twice for 1 min. Sections were dried on a hotplate at 60C before silver amplification with a powerful light-insensitive physical developer (Newman and Jasani 1998). Sections were counterstained with 0.1% aqueous safranin O and mounted in Gurr's neutral mountant.

Sections were examined on an Olympus BX51 light microscope (Olympus Optical; London, UK). Digital photomicrographs were acquired with a Zeiss Axiocam and Axiovision software (Carl Zeiss Vision; Hallbergmoos, Germany). Image processing was performed with Adobe Photoshop.

Results

Rat Mesothelium

Pleura. Mesothelial cells of the visceral pleura of the lung contained large numbers of vesicles that were equally distributed between the apical and basolateral surfaces. The majority of these stained strongly for caveolin-1 (Figure 1A). In some areas, very strong immunoreactivity was seen associated with dense foci of vesicles (Figure 1B).

Mesothelial cells overlying the diaphragm had a distribution of vesicles similar to that in the lung, although the numerical density was slightly less. The majority of vesicles stained strongly for caveolin-1 (Figure 1C). In contrast, mesothelium overlying the intercostal muscles had only moderate numbers of vesicles. These were predominantly apical in distribution, and only a small proportion of these were immunopositive (Figure 1D).

Pericardium. Mesothelial cells on the surface of the heart (visceral pericardium) contained very few vesi-

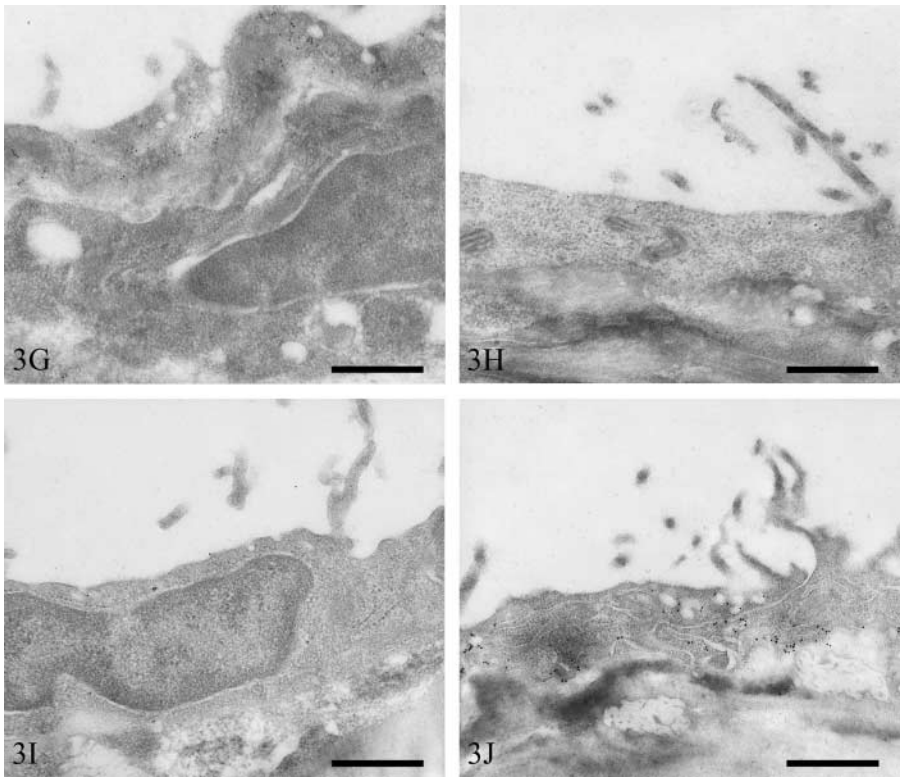

cles. Moderate numbers of these, however, stained positively for caveolin-1 (Figure 2A). In contrast, the parietal pericardial mesothelium contained very large numbers of vesicles, the majority of which stained strongly for caveolin-1 (Figure 2B).

Peritoneum. The subcellular distribution of vesicles fell into two broad categories, i.e., an equal distribution between the apical and basolateral surfaces and a predominantly apical distribution. A staining pattern of the former category was observed in mesothelial cells overlying the bladder, colon, kidney, and duodenum. Large numbers of vesicles were observed in both bladder (Figure 3A) and colon (Figure 3B) mesothelium, and vesicular immunostaining intensity was high in both. In contrast, both renal (Figure 3C) and duodenal (Figure 3D) mesothelium contained small numbers of vesicles, and few of these stained positively.

Mesothelial cells containing a predominantly apical distribution of vesicles occurred on the visceral peritoneum overlying the spleen, liver, mesentery, pancreas, and stomach. Mesothelial cells of the spleen (Figure 3E) and liver (Figure 3F) contained moderate numbers of vesicles. Only small numbers of splenic mesothelial vesicles stained positively for caveolin-1, whereas those of the liver were more numerously stained. Mesenteric (Figure 3G), pancreatic (Figure 3H), and gastric (Figure 3I) mesothelium contained low numbers of vesicles. Many vesicles of mesenteric mesothelium were positive for caveolin-1, whereas only moderate or low numbers were positive in pancreatic and gastric mesothelium, respectively.

Parietal peritoneal mesothelial cells of the abdominal wall contained moderate numbers of vesicles that were distributed equally between the apical and basolateral surfaces (Figure 3J). Moderate numbers of these were immunopositive for caveolin-1.

A summary of vesicular population density and intensity of immunostaining in the various mesothelial tissues is presented in Table 1. Differences in these parameters among the various sites were so obvious that only semiquantitative scoring was used.

Human Parietal Peritoneum

Light Microscopy. Semithin LR White resin sections afforded the highest optical resolution for light microscopy, because the entire thickness of the section was within the focal depth of the objective lens.

Caveolin-1 immuostaining localized to both the apical and basolateral surfaces of mesothelial cells, as well as intercellular junctions. Positive immunoreactivity was also observed in fibroblasts (Figure 4A). Venular and arteriolar vascular endothelium, and the smooth-muscle cells of arterioles, stained for caveo-

Table 1 Summary of vesicular density and labeling density at the different anatomic sites[a]

Tissue	Vesicular density	Immunolabeling density
Lung	+ + + + +	+ + + + +
Diaphragm	+ + + +	+ + + +
Intercostal muscle	+ + +	+
Heart	+	+ + +
Sac	+ + + + +	+ + + +
Bladder	+ + + +	+ + + +
Colon	+ + + +	+ + + +
Kidney	+	+ +
Duodenum	+	+ +
Spleen	+ + +	+
Liver	+ + +	+ + +
Mesentery	+ +	+ + + +
Pancreas	+	+ + +
Stomach	+ +	+ +
Abdominal wall	+ + +	+ + +

[a] +, very low; + +, low; + + +, moderate; + + + +, high; + + + + +, very high.

lin-1, as did cells of the epineurium (Figure 4B) and lymphatic endothelium (Figure 4C). No caveolin-1 immunoreactivity was seen in mast cells or nerve fibers.

Electron Microscopy. Mesothelial cell caveolin-1 immunolocalization was predominantly basolateral and was associated with some but not all vesicles (Figure 5A). Intercellular junctions had clusters of caveolin-1–positive vesicles (Figure 5B). Non-vesicular linear staining along the basolateral plasma membrane was also occasionally observed (Figure 5C). Within the submesothelial collagenous zone, strong caveolin-1–positive staining occurred in dense foci of vesicles in lymphatic endothelium (Figure 6A). Strong vesicular staining also occurred in vascular endothelium and smooth-muscle cells (Figure 6B). Epineural fibroblasts contained moderate numbers of caveolin-1–positive vesicles (Figure 6C).

Double immunolabeling with polyclonal anti-caveolin-1 and monoclonal anti-vimentin confirmed the specificity of caveolin-1 labeling. In endothelial cells, caveolin-1 (10-nm colloidal gold) localized to cytoplasmic and plasma membrane vesicles, whereas vimentin (20-nm colloidal gold) localized to cytoplasmic sites only (Figure 7A). In some areas of endothelium, foci of immunopositive vesicles were observed. These regions were completely devoid of vimentin staining (Figure 7B).

Discussion

Large numbers of vesicular structures within mesothelial cells have been observed and commented upon in a variety of animal species, including teleost fish (Leknes 1989), frogs (Hama 1960), mice (Casley-Smith 1969; Ettarh and Carr 1996), rats (Odor 1954; Wang 1974; Dobbie et al. 1981; Michailova and Vassilev 1985; Michailova, 1995,2001; Michailova et al. 1999), guinea pigs (Michailova and Vassilev 1988), rabbits (Baradi and Hope 1964; Obata 1978; Gotloib et al. 1983), cats (Michailova 1996), pigs (Pfeiffer et al. 1987), and humans (Dobbie et al. 1981; Di Paulo et al. 1986; Slater et al. 1989; Li et al. 1996; Michailova 1997). Such observations, made across several phyla, suggest that these vesicles are of fundamental importance to the biology of these cells.

A confusing number of terms have been used to describe these structures, such as pinocytotic vesicles (Baradi and Hope 1964; Obata 1978; Di Paulo et al. 1986; Pfeiffer et al. 1987; Leknes 1989), micropinocytotic vesicles (Dobbie et al. 1981; Dobbie 1989), pinocytic vesicles (Wang 1974), plasmalemmal vesicles (Shumko et al. 1993), microvesicles (Michailova 1995, 1997), and caveolae (Hama 1960; Slater et al. 1989; Ettarh and Carr 1996). Unlike clathrin-coated pits, which are easily identified by virtue of their characteristic electron-dense outer coating, it is much harder to discriminate between caveolae and similarly structured vesicles by morphological criteria alone. In this

Figure 4 Light micrographs of human parietal peritoneum immunostained for caveolin-1. **(A)** Mesothelium and fibroblasts (F). Bar = 10 μm. **(B)** Immunostaining of venules (V), arterioles (A) and nerves (N). Bar = 50 μm. **(C)** Immunostaining of lymphatic endothelium (L) and venule (V). Bar = 10 μm.

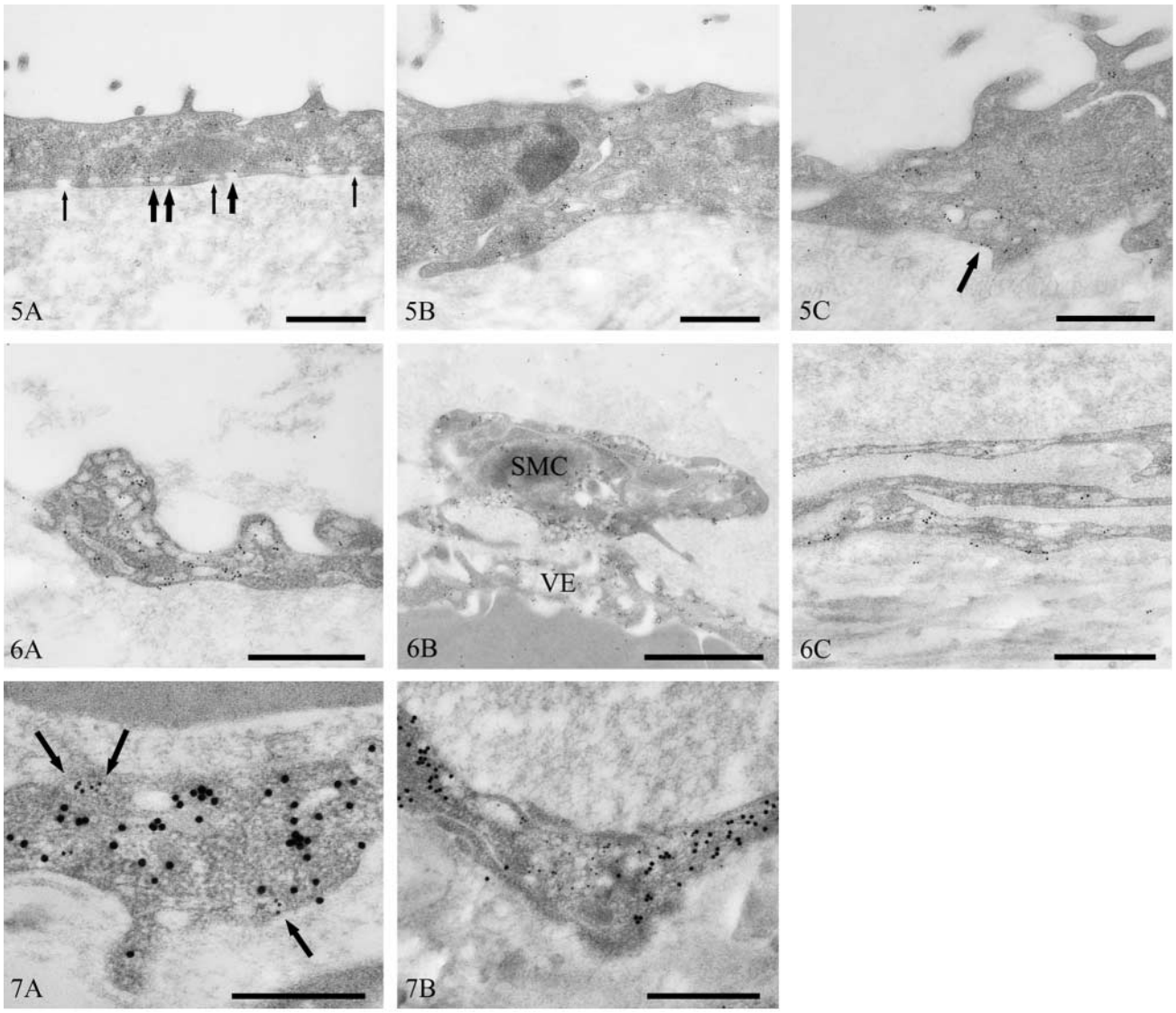

Figures 5–7

Figure 5 Transmission electron micrographs of human peritoneal mesothelium immunostained for caveolin-1. Immunopositive (thick arrows) and immunonegative (thin arrows) vesicles (**A**), clustering of immunopositive vesicles around an intercellular junction (**B**), and linear plasmalemmal staining (arrow) (**C**). Bars = 500 nm.

Figure 6 Transmission electron micrographs of human peritoneum immunostained for caveolin-1. Lymphatic endothelium (**A**), vascular endothelium (VE) and smooth-muscle cell (SMC) (**B**), and epineural fibroblasts (**C**). Bars = 500 nm.

Figure 7 Transmission electron micrographs of human peritoneal vascular endothelium immunostained for caveolin-1 and vimentin. Vesicular localization of caveolin-1 (10 nm immunogold) (arrows) and cytoplasmic localization of vimentin (20 nm immunogold) (**A**). Focus of caveolin-1–immunopositive vesicles (**B**). Bars = 500 nm.

article, we have sought to address this problem and to clarify the confusing nomenclature using an immunocytochemical approach.

The ICC localization of caveolin-1 to many of the flask-shaped 80–100-nm vesicular structures in mesothelial cells could be said to confirm that they are caveolae. However, some similarly structured vesicles did not immunolabel for caveolin-1. There are a number of possibilities to explain this. The failure of these vesicles to stain positively may be due to variations in caveolin-1 levels within caveolae, coupled with antigen threshold requirements. Similar observations have been made in type 1 pneumocytes (Newman et al. 1999). Alternatively, caveolae may contain caveolin-1 only at certain stages of their existence. It is also conceivable that caveolin-1 in some caveolae, although

being biochemically unaltered, undergoes conformational changes that render it immunocytochemically different. Finally, it may reflect genuine biochemical heterogeneity in morphologically similar structures.

Mesothelial cell caveolin-1 staining was highest in visceral pleura (lung) and parietal pericardium (pericardial sac). Variations in mesothelial cell vesicular density have been noted at a variety of sites in many animal species. For example, visceral pleural mesothelial cells have been consistently observed to contain larger numbers of vesicles than parietal cells, irrespective of species (Wang 1974; Obata 1978; Michailova and Vassilev 1985; Michailova, 1996,1997,2001). Similarly, within the peritoneal cavity, mesothelial cells overlying the spleen, bladder, rectum (Michailova 1995, 1996), and uterus (Odor 1954; Michailova 1995,1996) have been reported to have high numbers of vesicles, whereas those cells overlying the liver (Michailova 1995,1996) and omentum (Michailova, 1995,1996) have lower numbers. At other sites, some disagreement exists as to vesicular density. For example, abdominal wall mesothelial cells have been reported by some to have large numbers of vesicles (Baradi and Hope 1964; Obata 1978; Dobbie et al. 1981; Gotloib et al. 1983; Dobbie 1989), whereas others report low numbers (Slater et al. 1989; Michailova 1995,1996).

The variation in mesothelial caveolae density among different anatomic sites may have implications for understanding the development of certain diseases. For example, malignant mesothelioma is a rare but frequently fatal tumor that predominantly affects the pleura. Primary peritoneal lesions are less common, accounting for ~30% of cases (Moertel 1972), and primary pericardial tumors are extremely rare, with an incidence of less than 1% (Thomason et al. 1994). In 80% of all cases, the disease can be directly attributed to asbestos exposure (Attanoos and Gibbs 1997), which explains the preponderance of pleural tumors in these cases, because the pathway of asbestos fiber entry is invariably respiratory. In 20% of cases, however, no history of previous exposure to asbestos has been found.

In 1993, SV40 was reported to induce malignant mesothelioma in hamsters (Cicala et al. 1993). Interestingly, intrapleural administration induced malignant mesothelioma in 100% of animals, whereas IP injection resulted in only a 50% incidence. These observations mirror the incidence of primary pleural versus peritoneal malignant mesothelioma in humans. Subsequent investigations revealed that ~60% of human malignant mesothelioma specimens contained SV40 DNA sequences.

Between 1955 and 1963, poliovirus vaccine contaminated with SV40 was administered to over 90 million people in the United States. At the same time, 60% of the European population received similarly contaminated vaccine (Jasani et al. 2001). Not all European countries, however, initiated vaccination programs at this time. In those countries that began poliovirus vaccination after the contamination had been detected and eliminated, such as Turkey and Finland, no SV40 has been detected in malignant mesothelioma specimens (Hirvonen et al. 1999; De Rienzo et al. 2002).

Mesothelial cells are particularly susceptible to transformation by both asbestos and SV40. This susceptibility has been attributed to the higher levels of the tumor suppressor protein p53 in mesothelial cells than in, for example, fibroblasts, where SV40 infection leads to viral replication and cell lysis (Bocchetta et al. 2000).

Several lines of evidence indicate that the SV40 enters cells via caveolae, given that cells transfected with dominant-negative caveolin-1 (Roy et al. 1999) and cells treated with drugs, such as nystatin and filipin, that selectively disrupt the caveolar membrane system (Anderson et al. 1996) are sufficient to inhibit viral infection. The caveolar internalization of SV40 is unique, in that it utilizes novel transport intermediates that provide a direct route to the endoplasmic reticulum (ER), thereby bypassing the classic endosomal/lysosomal route and the Golgi complex. Furthermore, SV40 uptake proceeds at a much slower rate (hours as opposed to minutes) than the uptake of other viruses that utilize clathrin-coated pits. SV40 uptake is a multistep process that is initiated after binding of the SV40 particle to its cognate receptor, the MHC class I molecule, located on flattened regions of the cell membrane (Anderson et al. 1996,1998; Stang et al. 1997). At such sites, caveolin-1 is recruited to the plasma membrane and the SV40 virus elicits an extracellularly regulated and mitogen-activated protein kinase-independent intracellular signal that results in the enclosure and endocytosis of virons within small caveolae vesicles (Chen and Norkin 1999). These vesicles are targeted to larger caveolin-1–rich organelles termed caveosomes, from which they are sorted into tubular caveolin-1–free membrane vesicles and transported directly to the ER in a microtubule-dependent manner (Pelkmans et al. 2001).

This body of evidence suggests that SV40 might be one causative agent of malignant mesothelioma in humans. This issue, however, remains controversial, with some workers drawing attention to, for example, a number of technical problems associated with unequivocal virus identification, and the unexplained observations that SV40 DNA or protein is not found in all cells of a tumor (Garcea and Imperiale 2003).

When asbestos exposure or other factors have been eliminated as causes of malignant mesothelioma and if SV40 is a genuine carcinogen that has been inadvertently administered by an effectively systemic route, the

predominance of pleural versus peritoneal mesotheliomas may be due to a number of factors. For example, parietal pleural and pericardial blood flows have been measured at ten times those of parietal peritoneum (Townsley et al. 1991). Furthermore, in the few cases in which tumors are discovered during incidental surgery and the primary sites can be identified, these often occur at locations where caveolar density is high, such as the pericardium (Hirano et al. 2002), uterus, and bladder (Goldblum and Hart 1995). Mesothelial cells from different anatomic sites may vary in their susceptibility to transformation. The extremely low incidence of malignant mesothelioma of the pericardium, in spite of its anatomical proximity to the pleura, its similar blood flow, and its high density of caveolae (at least in the pericardial sac) suggests that this might be the case.

Osteosarcomas (Diamandopoulous 1972; Cicala et al. 1993) and ependymomas (Gerber and Kirschstein 1962) have also been observed in hamsters injected with SV40. Similar tumors in humans have been demonstrated to contain SV40 (Carbone et al. 1996; Zhen et al. 1999; Weggen et al. 2000; Yamamoto et al. 2000).

Recently, caveolae have been identified morphologically in osteoblasts (Solomon et al. 2000; Lofthouse et al. 2001). In addition, several studies have noted small numbers of vesicular structures in ependymal cells of the choroid plexus (Peters and Swan 1979; Madhavi and Jacob 1995), third ventricle (Ray and Choudhury 1984), and cerebral aqueducts (Meller and Dennis 1993) that may be caveolae.

Additional regions of high caveolar density within the peritoneal cavity (e.g., vascular and lymphatic endothelium, fibroblasts) may act as replication sites for SV40. Fibroblasts, for example, support SV40 replication (Bocchetta et al. 2000), and Sasaguri et al. (1991) reported that cultured aortic smooth-muscle cells were completely permissive to SV40 infection.

It is now well established that caveolin-1 can inhibit a number of signaling molecules whose phosphorylation, and hence activation, is required for cell growth and oncogenesis (Couet et al. 2001). Therefore, caveolin-1 has been proposed to represent the elusive tumor suppressor protein that is thought to reside at the 7q31.1 chromosomal locus and that is frequently deleted in a wide spectrum of human cancers (Engelman et al. 1998). The signaling intermediates known to be inhibited by direct interactions with caveolin-1 include the epidermal growth factor and platelet-derived growth factor receptor kinases, Neu tyrosine kinase, Ras, and components of the p42/p44 mitogen-activated cascade (Couet et al. 2001). Indeed, the caveolin-1 gene is transcriptionally repressed by activated p42/p44 (Engelman et al. 1999). It is noteworthy that both SV40 and asbestos fibers, two major causative agents in the development of malignant mesothelioma, stimulate p42/p44 within pleural mesothelial cells (Mossman and Gruenert 2002). Specifically, asbestos induces the upregulation and phosphorylation of EGF-R upstream of p42/p44 (Zanella et al. 1996), while the small T-antigen of the SV40 virus binds to and inhibits protein phosphatase 2A, a protein involved in the dephosphorylation and inactivation of p42/p44 (Rundell and Parakati 2001). Therefore, the loss of caveolin-1 and functional caveolae may represent an important step in the establishment of malignant mesothelioma. This hypothesis warrants investigation.

Vesicles in peritoneal mesothelial cells of patients exposed to the hyperosmotic environment of peritoneal dialysis (PD) are swollen compared with normal cells (Dobbie and Zaki 1986; Dobbie, 1989); this may be a common feature of the caveolar response to hypertonic environments. Acute osmotic shock causes internalization and swelling of cardiac myocyte caveolae (Kordylewski et al. 1993; Page et al. 1998) and internalization of caveolin-1 to a perinuclear location in fibroblasts (Kang et al. 2000), suggesting that caveolae may act as osmometers (Page et al. 1998).

Caveolin-1 is a non-competitive inhibitor of nitric oxide synthase (NOS) (Ju et al. 1997). Similarly, muscle-specific caveolin-3 has a similar effect on neuronal NOS (nNOS) (Venema et al. 1997), which has been identified in vascular smooth muscle (Cheah et al. 2002).

Elevated levels of both endothelial NOS and NOS activity have been noted in the peritoneum of patients on long-term PD (Combet et al. 2000; Devuyst et al. 2001).

It is conceivable that dissociation of caveolin-1 from caveolae in response to the hyperosmotic environment of PD reduces the normal allosteric inhibition of NOS, leading, at least in part, to the increased activity of NOS observed in long-term PD patients. Manipulation of peritoneal caveolae function may provide one approach to overcoming some of the undesirable side effects of long-term PD, such as loss of ultrafiltration, which has been associated with elevated NOS activity (Devuyst et al. 2001).

Acknowledgments

We are indebted to the Peritoneal Biopsy Study Group for supplying normal human peritoneal tissue.

Literature Cited

Anderson HA, Chen YZ, Norkin LC (1996) Bound simian virus 40 translocates to caveolin-enriched membrane domains, and its entry is inhibited by drugs that selectively disrupt caveolae. Mol Biol Cell 7:1825–1834

Anderson HA, Chen YZ, Norkin LC (1998) MHC class I molecules are enriched in caveolae but do not enter with simian virus 40. J Gen Virol 79:1469–1477

Anderson RGW (1999) Structure and function of caveolae. Biophys J 76:A31

Anderson RGW, Kamen BA, Rothberg KG, Lacey SW (1992) Potocytosis: sequestration and transport of small molecules by caveolae. Science 255:410–411
Attanoos RL, Gibbs AR (1997) Pathology of malignant mesothelioma. Histopathology 30:403–418
Baradi AF, Hope J (1964) Observations on ultrastructure of rabbit mesothelium. Exp Cell Res 34:33–44
Bocchetta M, Di Resta I, Powers A, Fresco R, Tosolini A, Testa JR, Pass HI, et al. (2000) Human mesothelial cells are unusually susceptible to simian virus 40-mediated transformation and asbestos carcinogenicity. Proc Natl Acad Sci USA. 97:10214–10219
Bretscher MS, Whytock S (1977) Membrane-associated vesicles in fibroblasts. J Ultrastruct Res 61:215–217
Carbone M, Pass HI, Rizzo P, Marinetti MR, Dimuzio M, Mew DJY, Levine AS, et al. (1994) Simian-virus 40-like DNA-sequences in human pleural mesothelioma. Oncogene 9:1781–1790
Carbone M, Rizzo P, Procopio A, Giuliano M, Pass HI, Gebhardt MC, Mangham C, et al. (1996) SV40-like sequences in human bone tumors. Oncogene 13:527–535
Casley-Smith JR (1969) The dimension and numbers of small vesicles in cells, endothelial and mesothelial and the significance of these for endothelial permeability. J Microsc 90:251–269
Cheah LS, Gwee MCE, Das R, Ballard H, Yang YF, Daniel EE, Kwan CY (2002) Evidence for the existence of a constitutive nitric oxide synthase in vascular smooth muscle. Clin Exp Pharmacol Physiol 29:725–727
Chen YZ, Norkin LC (1999) Extracellular simian virus 40 transmits a signal that promotes virus enclosure within caveolae. Exp Cell Res 246:83–90
Cicala C, Pompetti F, Carbone M (1993) Sv40 induces mesotheliomas in hamsters. Am J Pathol 142:1524–1533
Combet S, Miyata T, Moulin P, Pouthier D, Goffin E, Devuyst O (2000) Vascular proliferation and enhanced expression of endothelial nitric oxide synthase in human peritoneum exposed to long-term peritoneal dialysis. J Am Soc Nephrol 11:717–728
Couet J, Belanger MM, Roussel E, Drolet MC (2001) Cell biology of caveolae and caveolin. Adv Drug Deliv Rev 49:223–235
Craighead JE, Mossman BT (1982) The pathogenesis of asbestos-associated diseases. N Engl J Med 306:1446–1455
De Rienzo A, Tor M, Sterman DH, Aksoy F, Albelda SM, Testa JR (2002) Detection of SV40 DNA sequences in malignant mesothelioma specimens from the United States, but not from Turkey. J Cell Biochem 84:455–459
Devuyst O, Combet S, Cnops Y, Stoenoiu MS (2001) Regulation of NO synthase isoforms in the peritoneum: implications for ultrafiltration failure in peritoneal dialysis. Nephrol Dial Transpl 16: 675–678
Diamandopoulous GT (1972) Leukemia, lymphoma and osteosarcoma induced in the Syrian Golden hamster by simian virus 40. Science 176:173–175
Di Paulo N, Sacci G, De Mia M, Gaggiotti E, Capotondo L, Rossi P, Bernini M, (1986) Morphology of the peritoneal membrane during continuous ambulatory peritoneal dialysis. Nephron 44: 204–211
Dobbie JW (1989) Morphology of the peritoneum in CAPD. Blood Purification 7:74–85
Dobbie JW, Zaki MA (1986) The ultrastructure of the parietal peritoneum in normal and uraemic man and in patients on CAPD. In Maher JF, Winchester JF, eds. Frontiers in Peritoneal Dialysis. New York, Field, Rich, and Associates, 3–10
Dobbie JW, Zaki M, Wilson L (1981) Ultrastructural studies on the peritoneum with special reference to chronic ambulatory peritoneal dialysis. Scott Med J 26:213–223
Engelman JA, Zhang XL, Lisanti MP (1998) Genes encoding human caveolin-1 and -2 are co-localized to the D7S522 locus (7q31.1), a known fragile site (FRA7G) that is frequently deleted in human cancers. FEBS Lett 436:403–410
Engelman JA, Zhang XL, Razani B, Pestell RG, Lisanti MP (1999) p42/44 MAP kinase-dependent and -independent signaling pathways regulate caveolin-1 gene expression. Activation of Ras-MAP kinase and protein kinase a signaling cascades transcriptionally down-regulates caveolin-1 promoter activity. J Biol Chem 274:32333–32341
Ettarh RR, Carr KE (1996) Ultrastructural observations on the peritoneum in the mouse. J Anat 188:211–215
Fielding PE, Fielding CJ (1996) Intracellular transport of low density lipoprotein derived free cholesterol begins at clathrin-coated pits and terminates at cell surface caveolae. Biochemistry 35:14932–14938
Forbes MS, Rennels ML, Nelson E (1979) Caveolar systems and sacroplasmic reticulum in coronary smooth muscle cells of the mouse. J Ultrastruct Res 67:325–339
Garcea RL, Imperiale MJ (2003) Simian virus 40 infection of humans. J Virol 77:5039–5045
Gerber P, Kirschstein RL (1962) SV40-induced ependymomas in newborn hamsters. Virology 18:582–588
Glenney JR, Soppet D (1992) Sequence and expression of caveolin, a protein-component of caveolae plasma-membrane domains phosphorylated on tyrosine in rous-sarcoma virus-transformed fibroblasts. Proc Natl Acad Sci USA 89:10517–10521
Goldblum J, Hart WR (1995) Localized and diffuse mesotheliomas of the genital-tract and peritoneum in women. A clinicopathological study of 19 true mesothelial neoplasms, other than adenomatoid tumors, multicystic mesotheliomas, and localized fibrous tumors. Am J Surg Pathol 19:1124–1137
Gotloib L, Digenis GE, Rabinovich S, Medline A, Oreopoulos DG (1983) Ultrastructure of normal rabbit mesentery. Nephron 34: 248–255
Hama K (1960) The fine structure of the desmosomes in frog mesothelium. J Biophys Biochem Cytol 7:575–577
Hirano H, Maeda T, Tsuji M, Ito Y, Kizaki T, Yoshii Y, Sashikata T (2002) Malignant mesothelioma of the pericardium: Case reports and immunohistochemical studies including Ki-67 expression. Pathol Int 52:669–675
Hirvonen A, Mattson K, Karjalainen A, Ollikainen T, Tammilehto L, Hovi T, Vainio H, et al. (1999) Simian virus 40 (SV40)-like DNA sequences not detectable in Finnish mesothelioma patients not exposed to SV40-contaminated polio vaccines. Mol Carcinog 26:93–99
Holmes CJ (1994) Peritoneal host defence mechanisms in peritoneal dialysis. Kidney Int 46(suppl 48):58–70
Jasani B, Cristaudo A, Emri SA, Gazdar AF, Gibbs A, Krynska B, Miller C, et al. (2001) Association of SV40 with human tumours. Semin Cancer Biol 11:49–61
Ju H, Zou R, Venema VJ, Venema RC (1997) Direct interaction of endothelial nitric-oxide synthase and caveolin-1 inhibits synthase activity. J Biol Chem 272:18522–18525
Kang YS, Ko YG, Seo JS (2000) Caveolin internalization by heat shock or hyperosmotic shock. Exp Cell Res 255:221–228
Ke Y, Reddel RR, Gerwin BI, Reddel HK, Somers ANA, McMenamin MG, Laveck MA, et al. (1989) Establishment of a human in-vitro mesothelial cell model system for investigating mechanisms of asbestos-induced mesothelioma. Am J Pathol 134:979–991
Kordylewski L, Goings GE, Page E (1993) Rat atrial myocyte plasmalemmal caveolae in situ. Reversible experimental increases in caveolar size and in surface-density of caveolar necks. Circ Res 73: 135–146
Leknes IL (1989) Ultrastructure of the parietal pericardium in teleosts. J Anat 138:703–712
Li JC, Chen XB, Yu SM (1996) The ultrastructure of vesicle-containing cells and ER-cells of human peritoneum. Anat Anz 178: 365–367
Lofthouse RA, Davis JR, Frondoza CG, Jinnah RH, Hungerford DS, Hare JM (2001) Identification of caveolae and detection of caveolin in normal human osteoblasts. J Bone Joint Surg (Br) 83B:124–129
Madhavi C, Jacob M (1995) Light and electron-microscopic structure of choroid-plexus in hydrocephalic guinea pig. Indian J Med Res 101:217–224
Meller ST, Dennis BJ (1993) A scanning and transmission electron microscopic analysis of the cerebral aqueduct in the rabbit. Anat Rec 237:124–140

The Journal of Histochemistry & Cytochemistry

Michailova K, Wassilev W, Wedel T (1999) Scanning and transmission electron microscopic study of visceral and parietal peritoneal regions in the rat. Anat Anz 181:253–260
Michailova KM, Vassilev VA (1985) On the ultrastructure of the mesothelium in the pulmonary and parietal pleuras. Dokladi Bolgarsk Akad Nauk 38:263–266
Michailova KN (1995) A combined electron-microscopic investigation of the peritoneal mesothelium in the rat. Eur J Morphol 33: 265–277
Michailova KN (1996) The serous membranes in the cat. Electron microscopic observations. Anat Anz 178:413–424
Michailova KN (1997) Ultrastructural observations on the human visceral pleura. Eur J Morphol 35:125–135
Michailova KN (2001) Electronmicroscopic observations on the visceral and parietal rat's pleura after contralateral pneumonectomy. Eur J Morphol 39:47–56
Michailova KN, Vassilev VA (1988) On the ultrastructure of the mesothelium of the visceral pleura in the guinea-pig. Doklad Bolgarsk Akad Nauk 41:131–134
Moertel CG (1972) Peritoneal mesothelioma. Gastroenterology 63: 346–350
Mossman BT, Gruenert DC (2002) SV40, growth factors, and mesothelioma: another piece of the puzzle. Am J Respir Cell Mol Biol 26:167–170
Newman GR, Campbell L, von Ruhland C, Jasani B, Gumbleton M (1999) Caveolin and its cellular and subcellular immunolocalisation in lung alveolar epithelium: implications for alveolar epithelial type I cell function. Cell Tissue Res 295:111–120
Newman GR, Hobot JA (2001) Resin Microscopy and On-section Immunocytochemistry. Berlin, Heidelberg, New York, Springer-Verlag
Newman GR, Jasani B (1998) Silver development in microscopy and bioanalysis: a new versatile formulation for modern needs. Histochem J 30:635–645
Obata H (1978) Differences in normal structure and reaction to adjuvant between the costal and visceral pleura. Arch Histol Jpn 41:65–86
Odor DL (1954) Observations of the rat mesothelium with the electron and phase microscopes. Am J Anat 95:433–465
Page E, Winterfield J, Goings G, Bastawrous A, Upshaw-Earley J, Doyle D (1998) Water channel proteins in rat cardiac myocyte caveolae: osmolarity-dependent reversible internalization. Am J Physiology 43:H1988–2000
Pelkmans L, Kartenbeck J, Helenius A (2001) Caveolar endocytosis of simian virus 40 reveals a new two-step vesicular-transport pathway to the ER. Nat Cell Biol 3:473–483
Peters A, Swan RC (1979) The choroid plexus of the mature and aging rat: the choroidal epithelium. Anat Rec 194:325–353
Pfeiffer CJ, Pfeiffer DC, Misra HP (1987) Enteric serosal surface in the piglet. A scanning and transmission electron microscopic study of the mesothelium. J Submicrosc Cytol 19:237–246
Rajamannan NM, Springett MJ, Pederson LG, Carmichael SW (2002) Localization of caveolin 1 in aortic valve endothelial cells using antigen retrieval. J Histochem Cytochem 50:617–627
Ray PK, Choudhury SR (1984) Response of ependyma of the rat third ventricle to operative loss of cerebrospinal fluid: a transmission electron microscopical study. J Anat 138:513–523
Rothberg KG, Heuser JE, Donzell WC, Ying YS, Glenney JR, Anderson RGW (1992) Caveolin, a protein-component of caveolae membrane coats. Cell 68:673–682
Roy S, Luetterforst R, Harding A, Apolloni A, Etheridge M, Stang E, Rolls B, et al. (1999) Dominant-negative caveolin inhibits H-Ras function by disrupting cholesterol-rich plasma membrane domains. Nature Cell Biol 1:98–105
Rundell K, Parakati R (2001) The role of the SV40ST antigen in cell growth promotion and transformation. Semin Cancer Biol 11:5–13
Sasaguri Y, Yanagi H, Nagase H, Nakano R, Fukuda S, Morimatsu M (1991) Collagenase production by immortalized human aortic endothelial cells infected with simian virus-40. Virchows Arch [B] 60:91–97
Schnitzer JE, Oh P, Pinney E, Allard J (1994) Filipin-sensitive caveolae-mediated transport in endothelium: reduced transcytosis, scavenger endocytosis, and capillary-permeability of select macromolecules. J Cell Biol 127:1217–1232
Schlegel A, Lisanti MP (2001) Caveolae and their coat proteins, the caveolins: from electron microscopic novelty to biological launching pad. J Cell Physiol 186:329–337
Shin JS, Abraham SN (2001) Co-option of endocytic functions of cellular caveolae by pathogens. Immunology 102:2–7
Shumko JZ, Feinberg RN, Shalvoy RM, Defouw DO (1993) Responses of rat pleural mesothelia to increased intrathoracic pressure. Exp Lung Res 19:283–297
Simionescu N, Simionescu M (1983) The cardiovascular system. In Weiss L, ed. Histology: Cell and Tissue Biology. New York, Elsevier Biomedical, 371–433
Slater NJ, Raftery AT, Cope GH (1989) The ultrastructure of human abdominal mesothelium. J Anat 167:47–56
Smart EJ, Ying YS, Anderson RGW (1995) Hormonal regulation of caveolae internalization. J Cell Biol 131:929–938
Solomon KR, Adolphson LD, Wank DA, McHugh KP, Hauschka PV (2000) Caveolae in human and murine osteoblasts. J Bone Miner Res 15:2391–2401
Stang E, Kartenbeck J, Parton RG (1997) Major histocompatibility complex class I molecules mediate association of SV40 with caveolae. Mol Biol Cell 8:47–57
Thomason R, Schlegel W, Lucca M, Cummings S, Lee S (1994) Primary malignant mesothelioma of the pericardium. Case report and literature review. Tex Heart Inst J 21:170–174
Townsley MI, Negrini D, Ardell JL (1991) Regional blood flow to canine parietal pleura and internal intercostal muscle. J Appl Physiol 70:97–102
Venema VJ, Ju H, Zou R, Venema RC (1997) Interaction of neuronal nitric-oxide synthase with caveolin-3 in skeletal muscle. Identification of a novel caveolin scaffolding/inhibitory domain. J Biol Chem 272:28187–28190
von Ruhland CJ, Newman GR, Topley N, Williams JD (2003) Can trauma mimic pathology of the peritoneal membrane? Perit Dial Int. 5:428–433
Wang NS (1974) The regional difference of pleural mesothelial cells in rabbits. Am Rev Respir Dis 110:623–633
Weggen S, Bayer TA, von Deimling A, Reifenberger G, von Schweinitz D, Wiestler OD, Pietsch T (2000) Low frequency of SV40, JC and BK polyomavirus sequences in human medulloblastomas, meningiomas and ependymomas. Brain Pathol 10:85–92
Yamada E (1955) The fine structure of the gall bladder epithelium of the mouse. J Biophys Biochem Cytol 1:445–469
Yamamoto H, Nakayama T, Murakami H, Hosaka T, Nakamata T, Tsuboyama T, Oka M, et al. (2000) High incidence of SV40-like sequences detection in tumour and peripheral blood cells of Japanese osteosarcoma patients. Br J Cancer 82:1677–1681
Yoshimura N, Murachi T, Heath R, Kay J, Jasani B, Newman GR (1986) Immunogold electron microscopic localisation of calpain 1 in skeletal muscle of rats. Cell Tissue Res 244:265–270
Zanella CL, Posada J, Tritton TR, Mossman BT (1996) Asbestos causes stimulation of the extracellular signal-regulated kinase 1 mitogen-activated protein kinase cascade after phosphorylation of the epidermal growth factor receptor. Cancer Res 56:5334–5338
Zhen HN, Zhang X, Bu XY, Zhang ZW, Huang WJ, Zhang P, Liang JW, et al. (1999) Expression of the simian virus 40 large tumor antigen (Tag) and formation of Tag-p53 and Tag-pRb complexes in human brain tumors. Cancer 86:2124–2132

The Journal of Histochemistry & Cytochemistry